International Journal of Heat and Mass Transfer 61 (2013) 577–582

Contents lists available at SciVerse ScienceDirect

International Journal of Heat and Mass Transfer

journal homepage: www.elsevier.com/locate/ijhmt

A molecular dynamics study of effective thermal conductivity in nanocomposites

Zhiting Tian [a], Han Hu [b], Ying Sun [b,*]

[a] Department of Mechanical Engineering, Massachusetts Institute of Technology, Cambridge, MA 02139, USA
[b] Department of Mechanical Engineering and Mechanics, Drexel University, Philadelphia, PA 19104, USA

ARTICLE INFO

Article history:
Received 17 July 2012
Received in revised form 5 February 2013
Accepted 8 February 2013

Keywords:
Effective thermal conductivity
Non-equilibrium molecular dynamics simulation
Nanocomposites
Phonon transport

ABSTRACT

In this study, non-equilibrium molecular dynamics (NEMD) simulations are performed to determine the effective thermal conductivity of nanocomposites embedded with a variety of nanoparticles. The effects of orientation and arrangement of asymmetric nanoparticles, thermal property mismatch at the interface, interface density per unit volume of nanocomposite, and polydispersity of nanoparticles on the effective thermal conductivity of nanocomposites are investigated. Simulation results are compared with existing model predictions based on the effective medium approach. Results indicate that, with the same particle volume fraction, the nanocomposites that have a larger interfacial area perpendicular to heat flow or a larger interface density yield a smaller effective thermal conductivity. In addition, a larger mismatch at the interface between the host material and nanoparticle inclusions leads to a smaller effective thermal conductivity. Finally, it is found that the effective thermal conductivity of nanocomposites decreases with increasing polydispersity of embedded nanoparticles.

1. Introduction

Thermal properties of nanocomposites have become an area of great research interest in recent years owing to diverse applications of nanocomposites in thermal interface materials [1], thermoelectrics [2], thermal barrier materials [3], and solar cells [4]. The advances in synthesis and processing of nanocomposites necessitate a better understanding of the interfacial thermal transport between nanoparticles and host materials due to the importance of interfaces at the nanoscale.

It is well known that, the thermal conductivity of a semiconducting or insulating single crystal alloy is usually lower than the average of the thermal conductivities of the constituent materials [5]. The lowest thermal conductivity in crystalline solids is generally that of an alloy, called "alloy limit". However, the thermal conductivity of nanocomposites can even below the alloy limit [6]. The presence of nanoparticles provides an effective scattering mechanism for mid/long wavelength phonons that dominate heat conduction and contribute most to the thermal conductivity. Interface scattering and intrinsic scattering in phonon transport are the two mechanisms to create thermal resistance for heat flow in nanocomposites [4]. Intrinsic scattering, including isotropic scattering, defect scattering and electron–phonon scattering can be neglected for insulating materials in perfect lattice structures at low temperatures [6]. However, interface scattering plays an important role in nanocomposites, where the increased phonon collisions prevent the phonons with high energy in the hot region from moving to the cold region and vice versa. This results in a low heat transport, and consequently a low thermal conductivity [7].

Several models exist to estimate thermal properties of composite materials. For example, Nan et al. [8] developed a general effective medium approach (EMA) to obtain the effective thermal conductivity of arbitrary spheroidal particulate composites. It was found that the effective thermal conductivities are a function of particle size, shape, orientation distribution, volume fraction and thermal boundary resistance (i.e., the Kapitza resistance). However, the model of Nan et al. [8] did not take into account the increased interface scattering at the nanoscale. Minnich and Chen [9] derived a modified EMA model for spherical particulate nanocomposites, involving the interface density defined as the total surface area of nanoparticles per unit volume of the composite. This modification produced model predictions in good agreement with Monte Carlo (MC) simulations in terms of the effective thermal conductivity. Their results showed that the interface density dominated the effective thermal conductivity in nanocomposites, where the thermal boundary resistance played a critical role. Ordonez-Miranda et al. [10] extended the modified EMA model proposed by Minnich and Chen [9] for spheroidal inclusions. They showed that the shape and size dependence of thermal conductivity of nanocomposites are due to the collision cross section per unit volume of the particles and the mean distance that the energy carriers can travel inside the particles. Kim and Majumdar [11] calculated the scattering cross section of polydispersed spherical nanoparticles for different particle radii and incoming wave vectors. It was found that large size

* Corresponding author. Tel.: +1 215 895 1373; fax: +1 215 895 1478.
E-mail address: ysun@coe.drexel.edu (Y. Sun).

0017-9310/$ - see front matter © 2013 Elsevier Ltd. All rights reserved.
http://dx.doi.org/10.1016/j.ijheatmasstransfer.2013.02.023

distributions of spherical nanoparticles block a large range of phonon spectrum. The larger the mass difference between the host material and the spherical nanoparticle, the larger the scattering cross section.

Several numerical techniques have been implemented to determine thermal transport in nanocomposites. For example, Yang and Chen [12] calculated the effective thermal conductivity of periodic two-dimensional (2D) nanocomposites with square silicon nanowires in germanium utilizing MC simulations by solving the Boltzmann transport equation (BTE) for phonon transport. It was demonstrated that for a fixed silicon wire dimension, the lower the atomic percentage of germanium, the lower the effective thermal conductivity of the nanocomposites, different from the observation of macroscale composites. Jeng et al. [13] conducted MC simulations to study 3D phonon transport in nanocomposites using a gray-medium approach and showed that the effective thermal conductivity of nanocomposites can reach below the alloy limit [14]. Using non-equilibrium molecular dynamics (NEMD) simulations, Hegedus and Abramson [15] demonstrated that the presence of a nanoparticle was less influential in reducing thermal conductivity than the addition of a thin film.

Most studies on thermal conductivity of nanocomposites are only concerned with one or two aspects of nanoparticle properties. To the best of our knowledge, a thorough analysis on the diverse nanoparticle properties affecting the effective thermal conductivity of nanocomposites is lacking. In this paper, the NEMD simulations are performed to determine to what extent heat transfer is affected by the presence of nanoparticles in nanocomposites. The advantages of NEMD lie in its ability to account for arbitrary shapes and structures of the nanoparticle composites without making any assumptions or simplifications on frequency dependent thermal properties. The effects of the orientation and arrangement of asymmetric nanoparticles, the thermal property mismatch at the interface, the interface density per unit volume of the composites and the polydispersity of nanoparticles on the effective thermal conductivity of nanocomposites are investigated. The simulations are compared with predictions based on the EMA model of Nan et al. [8] and the modified EMA models of Minnich and Chen [9] and Ordonez-Miranda et al. [10].

2. Simulation procedure

The NEMD simulation is used in this study by imposing a constant heat flux over the nanocomposite material. A desired heat flux inside a face centered cubic (FCC) argon crystal of $80a$ (a is the lattice constant of argon at 20 K) in x and $5a$ in y and z directions respectively with its [1 0 0] direction oriented along the x axis. Here, x is the direction of heat flow, while y and z are directions perpendicular to heat flow. Periodic boundary conditions are employed in x, y and z directions. Four lattice layers at both ends of the domain are assigned as the hot region (heat source), while eight lattices in the middle are assigned to the cold region (heat sink). In between, there are regular regions of host material, with 32 lattices on either side of the heat sink. Rectangular prism shaped nanoparticles of different sizes are embedded in the regular region of the host material.

The atomic interactions of solid argon are described by the Lennard–Jones (L–J) potential given by

$$\phi_{LJ}(r_{ij}) = 4\varepsilon\left[\left(\frac{\sigma_{LJ}}{r_{ij}}\right)^{12} - \left(\frac{\sigma_{LJ}}{r_{ij}}\right)^{6}\right] \tag{1}$$

where r_{ij} is the distance between atoms i and j, $\varepsilon = 1.657 \times 10^{-21}$ J is the depth of the potential well and $\sigma_{LJ} = 3.4 \times 10^{-10}$ m is the equilibrium separation parameter. A cutoff distance of $2.5\sigma_{LJ}$ is used for force calculations. The time unit of the system is $\tau = \sigma(m/\varepsilon)^{0.5} = 2.155 \times 10^{-12}$ s. An open-source molecular dynamics simulator, LAMMPS [16], is used for all simulations. To relax the system, a constant NPT (N is atom number, P is pressure, T is temperature) ensemble is performed using the Nose/Hoover thermostat and barostat until the system reaches zero pressure after ~200,000 time steps of 0.001τ each. This is followed by a constant NVE (V is volume, E is total energy) ensemble to update position and velocity of each atom using the Verlet algorithm. Meanwhile, for every time unit τ, a fixed amount of heat $\Delta\varepsilon$ is added to the hot region while the same amount of heat is subtracted from the cold region to impose a constant heat flux along the x direction. After ~5,000,000 time steps of 0.001τ each, the system approaches steady state where the temperature profile is obtained by time averaging over 500,000 time steps.

The simulation cell along the heat flow direction is divided into slices with every four lattice layers per slice, and the temperature for each slice is calculated using

$$(T_{MD})_j = \frac{\left\langle \sum_{i=1}^{N_j} m_i v_i^2 \right\rangle}{3N_j k_B} \tag{2}$$

where $\langle\rangle$ denotes statistical averaging over the simulation time, k_B is the Boltzmann constant, N_j is the atomic number in jth slice, m_i and v_i are the mass and velocity of the ith atom respectively, and $(T_{MD})_j$ is the temperature in the jth slice. The temperature gradient along x direction, dT/dx, for a pure material can be obtained from the temperature profile. This is the classical calculation, generally applied to high temperature limit compared to the Debye temperature. However, in this paper, solid argon with L–J potential is selected as the model material where the quantum effects are not expected to be significant [17,18]. Therefore, no quantum corrections are employed at low temperatures.

The heat flux J along the direction of heat flow (x-direction) can be calculated by

$$J_x = \frac{\Delta\varepsilon}{L_y L_z \Delta t} \tag{3}$$

where L_y and L_z are the sizes along y- and z-directions. For nanocomposites at steady-state where the temperature profiles are nonlinear, the effective thermal conductivity can be calculated using [15]

$$K^* = \frac{J_x}{\Delta T/\Delta x} \tag{4}$$

where ΔT is the temperature difference across a distance Δx. The effective thermal conductivity, K^*, of nanocomposites is calculated based on five independent runs for each case to determine to what extent it is affected by the shape, orientation, arrangement, thermal property, and polydispersity of embedded nanoparticles.

3. Models for effective thermal conductivity of nanocomposites

For composites containing equisized spheroidal inclusions, the effective thermal conductivities, K_{ii}^*, along the material axis X_i ($i = 1, 2, 3$) based on the EMA model of Nan et al. [8] is given by

$$\begin{aligned} K_{11}^* = K_{22}^* &= K_m \frac{2+f\left[\beta_{11}(1-L_{11})(1+\langle\cos^2\theta\rangle)+\beta_{33}(1-L_{33})\left(1-\langle\cos^2\theta\rangle\right)\right]}{2-f\left[\beta_{11}L_{11}\left(1+\langle\cos^2\theta\rangle\right)+\beta_{33}L_{33}(1-\langle\cos^2\theta\rangle\right]} \\ K_{33}^* &= K_m \frac{1+f\left[\beta_{11}(1-L_{11})\left(1-\langle\cos^2\theta\rangle\right)+\beta_{33}(1-L_{33})\langle\cos^2\theta\rangle\right]}{1-f\left[\beta_{11}L_{11}\left(1-\langle\cos^2\theta\rangle\right)+\beta_{33}L_{33}\langle\cos^2\theta\rangle\right]} \end{aligned} \tag{5}$$

where K_m is the bulk thermal conductivity of the matrix phase, f is the volume fraction of particles, the parameter $\beta_{ii} = \frac{K_{ii}^c - K_m}{K_m + L_{ii}(K_{ii}^c - K_m)}$, K_{ii}^c is the equivalent thermal conductivity along the X_i' symmetric axis of the spheroidal composite unit cell, L_{ii} is the particle shape

dependent parameter, $\langle\cos^2\theta\rangle = \frac{\int\rho(\theta)\cos^2\theta\sin\theta d\theta}{\int\rho(\theta)\sin\theta d\theta}$, θ is the angle between the materials axis X_3 and the local particle symmetric axis X_3', and $\rho(\theta)$ is a distribution function describing spheroidal particle orientation. Here, K_{ii}^c can be calculated using $K_{ii}^c = k_p/(1+\gamma L_{ii}k_p/k_m)$, where K_p is the bulk thermal conductivity of the spheroidal particle, $p = a_3/a_1$ is the particle aspect ratio, a_1 and a_3 are, respectively, radii of the spheroid along the X_1' and X_3' axes. For the case of $p \geqslant 1$ and $a_1 = a_2 < a_3$, $L_{11} = L_{22} = p^2/[2(p^2-1)] - p\cosh^{-1}p/[2(p^2-1)^{3/2}]$, $L_{33} = 1 - 2L_{11}$, $\gamma = (2+1/p)\alpha$, $\alpha = R_{Bd}K_m/a_1$, where R_{Bd} is the thermal boundary resistance. For composites with equisized spherical particles, the effective thermal conductivity of spheroids, Eq. (5), reduces to

$$K^* = K_m\frac{K_p(1+2\alpha)+2K_m+2f[K_p(1-\alpha)-K_m]}{K_p(1+2\alpha)+2K_m-f[K_p(1-\alpha)-K_m]} \tag{6}$$

Taking into account the increased interface scattering in nanocomposites, the modified EMA model of Minnich and Chen [9] for the effective thermal conductivity of nanocomposite gives

$$K^* = \frac{1}{3}C_m v_m\frac{1}{(1/\Lambda_m)+(\Phi/4)} \times\frac{K_p'(d)(1+2\alpha(\Phi,d))+2K_m'(\Phi)+2(\Phi d/6)\left[K_p'(d)(1-\alpha(\Phi,d)-K_m'(\Phi)\right)]}{K_p'(d)(1+2\alpha(\Phi,d))+2K_m'(\Phi)-(\Phi d/6)[K_p'(d)(1-\alpha(\Phi,d)-K_m'(\Phi))]} \tag{7}$$

where C is the volumetric specific heat, v the phonon group velocity, Λ is the phonon mean free path, Φ is the interface density, $K_p' = K_p/(1+\Lambda_p\Phi/4)$ and $K_m' = K_m/(1+\Lambda_m/d)$ are modified thermal conductivities of the particle and the host, respectively, and d is the particle diameter. For nanocomposites with spheroidal inclusions, Ordonez-Miranda et al. [10] introduced size- and shape-dependent thermal conductivities to replace the bulk thermal conductivities in the model of Nan et al. [8]. The resulting modified thermal conductivities of the particle and the host are given by $K_p'' = K_p/(1+\Lambda_p/c)$ and $K_m'' = K_m/(1+\Lambda_m\sigma_\perp f)$, respectively. Here, c is the average distance traveled by the energy carrier due to the scattering at the particle boundaries and $\sigma_\perp$ is the collision cross section per unit volume of the particles.

In the following, the effective thermal conductivities of nanocomposites calculated from molecular dynamics simulations are compared with model predictions of Nan et al. [8], Minnich and Chen [9], and Ordonez-Miranda et al. [10].

4. Results and discussion

4.1. Interfacial area perpendicular to heat flow

A nanoparticle of $2a$ in x, $2a$ in y, and $4a$ in z ($2a\times2a\times4a$, named NP224) is embedded at the center between the hot and cold zones (i.e., $x = 19a$–$21a$ and $59a$–$61a$) of a $80a\times5a\times5a$ host material and the calculated effective thermal conductivity is compared with that of the nanocomposite consisting of a nanoparticle of $4a\times2a\times2a$ (named NP422) embedded at $x = 18a$ - $22a$ and $58a$ - $62a$. The two nanoparticles have exactly the same volume, total surface area, and mass (four times that of the argon host), but different interfacial areas perpendicular to heat flow. The temperature profiles for these two cases are shown in Fig. 1. For both cases, larger temperature drops occur around the nanoparticles compared to that of the host material, indicating smaller thermal conductivity in the nanoparticle phase. The effective thermal conductivity of nanocomposite consisting of NP224 obtained by averaging five simulation runs is $K^*_{NP224} = 0.7318\ W/(m\cdot K)$ and that for the NP422 case is $K^*_{NP422} = 0.7725\ W/(m\cdot K)$, which yields a ratio of $K^*_{NP422}/K^*_{NP224} = 1.056$. Since all other parameters for the two cases are kept the same, a larger effective thermal conductivity for the NP422 case is the result of a smaller interfacial area perpendicular to the heat flow compared to that of NP224.

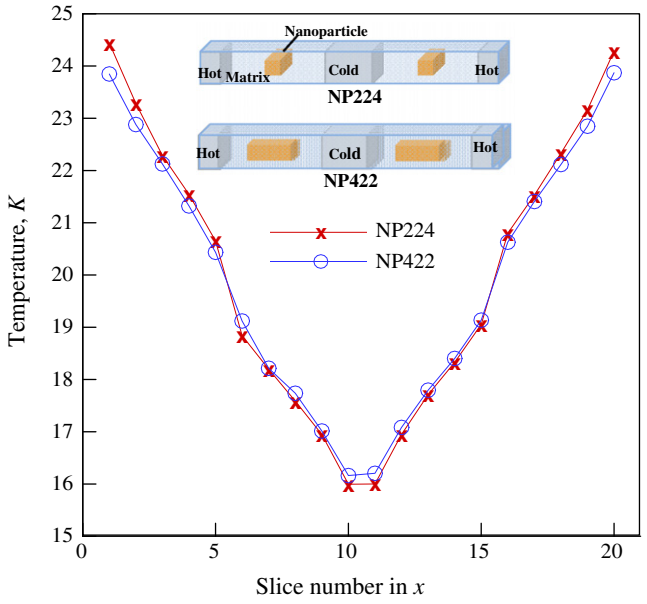

Fig. 1. Temperature profiles for nanocomposites of $80a\times5a\times5a$ embedded with a $2a\times2a\times4a$ nanoparticle and a $4a\times2a\times2a$ nanoparticle at 20 K and $J = 0.31\times10^9\ W/m^2$.

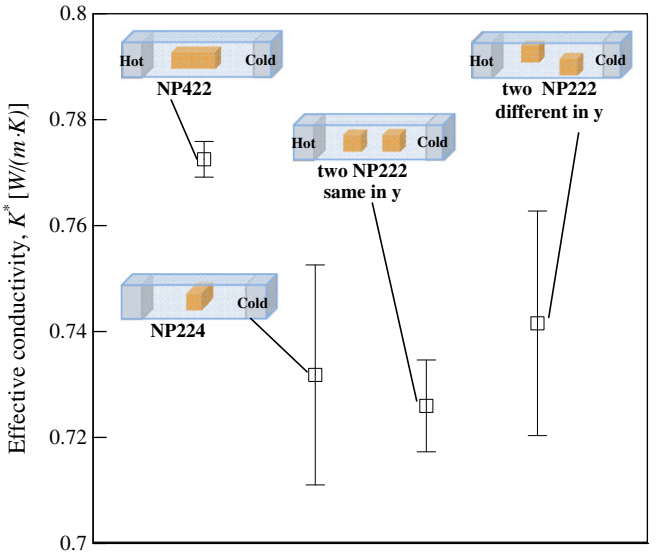

Fig. 2. Comparison of the effective thermal conductivities for nanocomposites embedded with a $4a\times2a\times2a$ nanoparticle, a $2a\times2a\times4a$ nanoparticle, two $2a\times2a\times2a$ nanoparticles of the same height, and two $2a\times2a\times2a$ nanoparticles of different height locations at 20 K and $J = 0.31\times10^9\ W/m^2$. Effective thermal conductivities are calculated from averaging five simulation runs and the error bar are the standard deviations.

The arrangement of nanoparticles in the composite is examined by comparing two nanoparticles of $2a\times2a\times2a$ (NP222) of the same height location vs. different height locations perpendicular to heat flow. Other properties and the separation distance between the two nanoparticles in the heat flow direction are kept the same. As shown in Fig. 2, the difference in the calculated effective thermal conductivities for these two cases is within the range of error. This implies that as far as the interfacial area perpendicular to heat

flow remains the same, the height location and the horizontal distance of the nanoparticles are not important provided that the volume fractions of the nanoparticles are keep the same. It is also interesting to note that the effective thermal conductivities for both the two NP222 cases are the same as the NP224 case, which implies that the interfacial area parallel to heat flow is less important in affecting the thermal properties of nanocomposites.

This observation is consistent with the mechanism of phonon propagation. Consider heat conduction along x, where the x-component of phonon group velocity, v_x, contributes to the heat flux. Phonons traveling parallel or quasi-parallel to the x-direction are the major contributors to heat conduction. While the interface perpendicular to heat flow effectively reduces the mean free paths of these phonons, the interface parallel to heat flow does not have a significant impact on these phonons. As a result, a larger area perpendicular to heat flow leads to a smaller thermal conductivity. An analogy to this is a higher in-plane thermal conductivity of an in-plane superlattice than that of a cross-plane superlattice [19,20], where the cross-plane interface is more efficient in phonon scattering [12]. We have also shown, using the phonon wave-packet method, the orientation of anisotropic nanocomposites is important in affecting the effective thermal conductivity [21].

To further investigate the effect of particle orientation on the effective thermal conductivity of the nanocomposite, the phonon spectra of the NP224 and NP422 nanocomposites are shown in Fig. 3. Here, the phonon density of states is calculated using the Fourier transform of the velocity auto-correlation functions of the atoms in the matrix and the particle. Since only 2% of the atoms are inside the particle and the interface mismatch between the matrix and particle are the same for both NP224 and NP422 cases, the effective thermal conductivities of the nanocomposites are predominantly determined by the phonon transport in the matrix. As shown in Fig. 3, the phonon spectra in the matrix for both NP422 and NP224 cases are very similar but the NP422 case has slightly larger phonon density of states at low frequencies around 0.6 THz. These lower frequency phonons have larger phonon mean free paths and contribute more to thermal transport, resulting in a higher effective thermal conductivity of the NP422 case.

By using a spheroid and a cylinder of the same aspect ratio and volume fraction to approximate rectangular prism shaped nanoparticles, the NEMD calculations can be compared with the EMA model for composites with spheroidal nanoparticles of Nan et al. [8] and the modified EMA model of Ordonez-Miranda et al. [10],

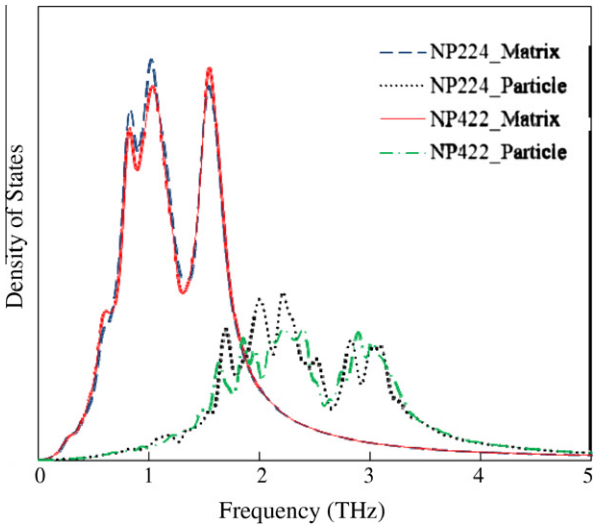

Fig. 3. Comparison of the phonon spectra of the nanocomposites embedded with a $4a \times 2a \times 2a$ nanoparticle, and a $2a \times 2a \times 4a$ nanoparticle, at 20 K.

respectively. The ratios of effective thermal conductivities based on NEMD simulations and the corresponding model predictions are summarized in Table 1. It is shown that the simulation result of $K^*_{\mathrm{NP422}}/K^*_{\mathrm{NP224}} = 1.056$ is very close to that of 1.066 predicted by the model of Ordonez-Miranda et al. [10] compared to $K^*_{\mathrm{NP422}}/K^*_{\mathrm{NP224}} = 1.023$ using the model of Nan et al. [8].

4.2. Interface density

Consider nanocomposites consisting of eight $2a \times 2a \times 2a$ nanoparticles and one $4a \times 4a \times 4a$ nanoparticle, respectively. For both cases, the total volume of the particulate phase is the same and the mass of nanoparticles is 0.25 times that of argon. The calculated effective thermal conductivity for the case of eight $2a \times 2a \times 2a$ nanoparticles is $K^*_{8-222} = 0.8090\ \mathrm{W/(m \cdot K)}$ and that of the one $4a \times 4a \times 4a$ case is $K^*_{444} = 0.8380\ \mathrm{W/(m \cdot K)}$ with the ratio $K^*_{444}/K^*_{8-222} = 1.036$, i.e., a larger interfacial area leads to a smaller effective thermal conductivity. It has been shown by Minnich and Chen [9] that the interface density is a primary factor in determining the effective thermal conductivity. The effective thermal conductivity decreases with decreasing particle size for a given particle volume fraction [6]. Since all nanoparticles are of cubic shape, comparing two nanocomposites with the same volume fraction, the smaller the particle size, the larger the interface density. The increased interface scattering due to smaller particle inclusions results in a smaller effective thermal conductivity.

To compare the NEMD calculations with the EMA model for spherical particles of Nan et al. [8] and the modified EMA models of Minnich and Chen [9] and Ordonez-Miranda et al. [10], the equivalent particle diameter for the same volume fraction as a cubic particle of size a is $d = (6/\pi)^{1/3}a \approx 1.24a$. Using the EMA model of Nan et al. [8], i.e., Eq. (5), the ratio of thermal conductivities between the nanocomposite with one $4a \times 4a \times 4a$ (NP444) nanoparticle and eight $2a \times 2a \times 2a$ nanoparticles is $(K^*_{444}/K^*_{8-222})_{\mathrm{Nan}} = 1.002$. This implies that the model of Nan et al. [8] fails to predict the difference in the effective thermal conductivity caused by different interface densities. Based on the modified EMA model of Minnich and Chen [9], i.e., Eq. (6), it follows $(K^*_{444}/K^*_{8-222})_{\mathrm{MC}} = 1.120$, compared to the ratio of 1.036 in the present NEMD simulation. Here, at the temperature of 20 K, the phonon mean free path in argon solid is $\Lambda_h = 75.285$ Å, calculated based on Choi et al. [7] The approximation of the average phonon mean free path and the fact that phonon mean free paths are strongly mode-dependent are believed to be the reasons for overestimating the effective conductivity ratio when using the model of Minnich and Chen [9]. Nevertheless, both the NEMD simulation and model prediction indicate that, for the same volume fraction, a larger interface density causes a smaller effective thermal conductivity of nanocomposites. The effective thermal conductivities based on NEMD simulation and the corresponding model predictions are summarized in Table 1.

4.3. Interface mismatch

Interface mismatch is examined using nanoparticles of $4a \times 4a \times 4a$ in size embedded into the central region ($18a$–$22a$ and $58a$–$62a$ in x) of a $80a \times 5a \times 5a$ host material. The mass of the nanoparticles varies from 0.0625, 0.125, 0.25, to 0.5. The results in Fig. 4 show that, the larger the mass mismatch, the smaller the effective thermal conductivity, which ranges from 0.6767 to 0.8749 W/(m · K). It is well known that the interface mismatch leads to a Kapitza resistance. From a wave transport perspective, the reflection of phonons at the interface reduces the number of forward-going phonons and thus creates thermal resistance. The phonon transmission coefficient at the interface can be estimated using the acoustic mismatch model (AMM) [23] or the diffuse mismatch model (DMM) [24]. For a perfectly smooth interface at

Table 1
Comparison of NEMD calculated effective thermal conductivities of nanocomposites with theoretical models.

Cases	Ratio of effective thermal conductivity, K_1^*/K_2^*			
	Based on Nan et al. [8]	Based on Minnich and Chen [9]	Based on Ordonez-Miranda et al. [10]	MD simulation (this study)
NP422 vs. NP224	1.023	N/A*	1.066	1.056
NP444 vs. 8 NP222s	1.002	1.120	1.120	1.036

* The model of Minnich and Chen [9] is only for spherical nanocomposites.

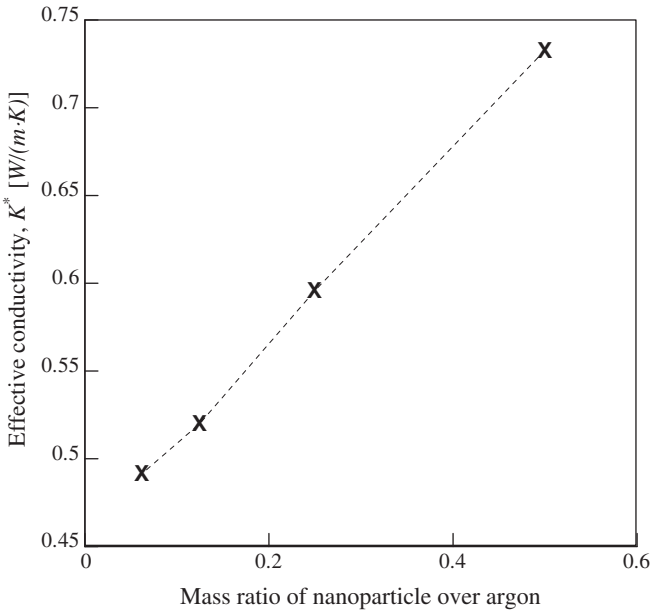

Fig. 4. Effective thermal conductivities for nanocomposites of different mass ratios. The host material keeps the same while the mass of the nanoparticle varies from 0.0625, 0.125, to 0.25 and 0.5. The simulations are conducted at 20 K and $J = 0.31 \times 10^9$ W/m^2.

a low temperature of 20 K as investigated in this study, AMM that assumes purely specular reflection and transmission provides a good description of the phonon transport across the interface. As the phonon acoustic impedance increases with the interface mismatch, the transmission coefficient decreases and the Kapitza resistance increases. In the present study, since the mass of the host material is kept at one, a smaller mass of nanoparticles leads to a larger interface mismatch, and hence a larger Kapitza resistance. At a higher temperature and for a rough interface, DMM that assumes purely diffuse scattering leads to a better prediction of interfacial phonon transport. As the interface mismatch increases, the mismatch in phonon density of states of the two materials across the interface becomes more profound, resulting in a lower transmission coefficient and thus a larger Kapitza resistance. It is therefore expected that the interface mismatch determines the Kapitza resistance over a variety of interfaces across a wide temperature range and is a critical factor for the effective thermal conductivity of nanocomposites with a large interfacial area between embedded nanoparticles and the host material.

Two competing factors exist as the mass of the nanoparticles decreases: higher bulk thermal conductivities of the nanoparticles which leads to lower resistance in the particle phase and the increase of Kaptiza resistance at the interface between nanoparticles and the host. The results indicate that the Kaptiza resistance is dominant in determining the effective thermal conductivity. Even though the nanoparticles have a much higher thermal conductivity than that of the host, the nanoparticle inclusions may not increase the effective thermal conductivity. In many nanocomposite materials, it is observed that the effective thermal conductivity decreases considerably with an increase of the Kapitza resistance [22] especially when the size of nanoparticles is small and the Kapitza resistance is considerably high.

Compared with the thermal conductivity of pure argon under the same conditions, $k = 1.0378$ W/(m · K), the effective thermal conductivities for all nanocomposites of different interface mismatch shown in Fig. 4 are smaller. It shows that, although the nanoparticle inclusions have a larger conductivity than the host material, the effective thermal conductivity of the nanocomposite do not exceed that of pure argon. Tian and Yang [4] observed that the effective thermal conductivity in compact silicon nanowire mixtures is considerably smaller than the single crystal bulk silicon because the interface scattering creates additional thermal resistance to heat flow. Moreover, if the nanoparticle has an energy parameter different from the host material, the effective thermal conductivity is also smaller than that of the pure material. The effectiveness of lattice mismatch highlights the significance of the Kaptiza resistance in determining the effective thermal conductivity of nanocomposites.

4.4. Polydispersity

The effect of polydispersity of nanoparticles on the effective thermal conductivity of nanocomposite is examined for the cases with the same average particle size but different size distributions. Two cases are considered, one with two embedded nanoparticles of $2a \times 2a \times 2a$ in a $80a \times 5a \times 5a$ host and the other with one $a \times a \times a$ (NP111) and one $3a \times 3a \times 3a$ (NP333) embedded nanoparticles, all with mass of 0.25 time that of argon. For both cases, the average particle size is $2a$, while the standard deviations are 0 and $1.41a$ respectively. The calculated effective thermal conductivities are $K^*_{2-222} = 0.8293$ W/(m · K) and $K^*_{111+333} = 0.7371$ W/(m · K), respectively, with a ratio of $K^*_{2-222}/K^*_{111+333} = 1.125$. It indicates that the larger particle size distribution (or polydispersity), the lower the effective thermal conductivity. The particles are most visible to the phonons with wavelength comparable to the particle size. If the particle size is smaller than the phonon wavelength, phonons will travel through it as if the particle does not exist. For particles with different sizes, phonons with a large range of wavelengths will be influenced. The resulting phonon scattering with particles leads to a resistance to heat flow. The conclusion obtained here is consistent with that of Kim and Majumdar [11], i.e., a large size distribution of spherical nanoparticle prevents effective transport of a larger range of phonon spectrum, which results in a larger scattering efficiency and a smaller effective thermal conductivity. This conclusion should also hold for cubic nanoparticles as it has been recently showed that approximating a square nanowire as a circular one of equal cross-sectional area is a very good approximation from the thermal property viewpoint [25].

In the present simulation, the two $2a \times 2a \times 2a$ nanoparticles strongly scatter phonons of one wavelength, while the case with one $a \times a \times a$ and one $3a \times 3a \times 3a$ nanoparticles blocks phonons of two different wavelengths. Despite a simple representation of polydispersity, the result shows that the polydispersity decreases the effective thermal conductivity. It will be more evident if there

is no computational limit and the simulation domain can be large enough to have more nanoparticles of different sizes.

5. Conclusion

In this study, NEMD simulations are performed to determine the effective thermal conductivity of nanocomposites. The effects of asymmetric nanoparticle orientation and arrangement, thermal property mismatch at the interface, the interface density per unit volume of nanocomposites and polydispersity of nanoparticles on the effective thermal conductivity are investigated. The simulated results are compared with the EMA model of Nan et al. [8] and the modified EMA models of Minnich and Chen [9] and Ordonez-Miranda et al. [10] Results indicate that, with the same volume fraction, the nanocomposites that have a larger interfacial area perpendicular to heat flow or a larger interface density yield a smaller effective thermal conductivity. In addition, interface mismatch plays an important role in determining the effective thermal conductivity. Finally, a larger polydispersity leads to a smaller effective thermal conductivity. These guidelines will help design nanocomposites with desired thermal properties.

Acknowledgments

This work was supported in part by the Integrated Electronic Engineering Center at the State University of New York at Binghamton and the U.S. National Science Foundation under Grant No. DMR-1104835. The authors also wish to thank NYSTAR for providing computational resources at the Computational Center for Nanotechnology Innovations.

References

[1] R. Prasher, Thermal interface materials: historical perspective, status, and future directions, Proc. IEEE 94 (2006) 1571–1586.
[2] M.S. Dresselhaus, G. Chen, M.Y. Tang, R.G. Yang, H. Lee, D.Z. Wang, Z.F. Ren, J.P. Fleurial, P. Gogna, New directions for low-dimensional thermoelectric materials, Adv. Mater. 19 (2007) 1043–1053.
[3] R.M. Costescu, D.G. Cahill, F.H. Fabreguette, Z.A. Sechrist, S.M. George, Ultra-low thermal conductivity in W/Al2O3 nanolaminates, Science 303 (2004) 989–990.
[4] W.X. Tian, R.G. Yang, Thermal conductivity modeling of compacted nanowire composites, J. Appl. Phys. 101 (2007) 054320.
[5] G.P. Srivastava, The Physics of Phonons, Taylor & Francis, 1990.
[6] K.M. Katika, L. Pilon, The effect of nanoparticles on the thermal conductivity of crystalline thin films at low temperatures, J. Appl. Phys. 103 (2008) 114308.
[7] S.-H. Choi, S. Maruyama, K.-K. Kim, J.-H. Lee, Evaluation of the phonon mean free path in thin films by using classical molecular dynamics, J. Korean Phys. Soc. 43 (2003) 747–753.
[8] C.W. Nan, R. Birringer, D.R. Clarke, H. Gleiter, Effective thermal conductivity of particulate composites with interfacial thermal resistance, J. Appl. Phys. 81 (1997) 6692–6699.
[9] A. Minnich, G. Chen, Modified effective medium formulation for the thermal conductivity of nanocomposites, Appl. Phys. Lett. 91 (2007) 073105.
[10] J. Ordonez-Miranda, R. Yang, J.J. Alvarado-Gil, On the thermal conductivity of particulate nanocomposites, Appl. Phys. Lett. 98 (2011) 233111.
[11] W. Kim, A. Majumdar, Phonon scattering cross section of polydispersed spherical nanoparticles, J. Appl. Phys. 99 (2006) 084306.
[12] R. Yang, G. Chen, Thermal conductivity modeling of periodic two-dimensional nanocomposites, Phys. Rev. B69 (2004) 195316.
[13] M.-S. Jeng, R. Yang, D. Song, G. Chen, Modeling the thermal conductivity and phonon transport in nanoparticle composites using Monte Carlo simulation, J. Heat Transfer 130 (2008) 042410.
[14] W. Kim, J. Zide, A. Gossard, D. Klenov, S. Stemmer, A. Shakouri, A. Majumdar, Thermal conductivity reduction and thermoelectric figure of merit increase by embedding nanoparticles in crystalline semiconductors, Phys. Rev. Lett. 96 (2006) 045901.
[15] P.J. Hegedus, A.R. Abramson, A molecular dynamics study of interfacial thermal transport in heterogeneous systems, Int. J. Heat Mass Transfer 49 (2006) 4921–4931.
[16] S. Plimpton, Fast parallel algorithms for short-range molecular dynamics, J. Comput. Phys. 117 (1995) 1–19.
[17] A.J.H. McGaughey, M. Kaviany, Thermal conductivity decomposition and analysis using molecular dynamics simulations. Part I. Lennard–Jones argon, Int. J. Heat Mass Transfer 47 (2004) 1783–1798.
[18] J. Che, T. Cagin, W. Deng, W.A. Goddard III, Thermal conductivity of diamond and related materials from molecular dynamics simulations, J. Chem. Phys. 113 (2000) 6888–6900.
[19] G. Chen, Size and interface effects on thermal conductivity of superlattices and periodic thin-film structures, J. Heat Transfer 119 (1997) 220–229.
[20] G. Chen, Thermal conductivity and ballistic-phonon transport in the cross-plane direction of superlattices, Phys. Rev. B57 (1998) 14958–14973.
[21] Z. Tian, S. Kim, Y. Sun, B.E. White, A molecular dynamics study of thermal conductivity in nanocomposites via the phonon wave packet method, in: Proceedings of the InterPACK '09, IPACK2009-89272, San Francisco, CA, 2009.
[22] H.M. Yin, G.H. Paulino, W.G. Buttlar, L.Z. Sun, Effective thermal conductivity of functionally graded particulate nanocomposites with interfacial thermal resistance, J. Appl. Mech. 75 (2008) 051113.
[23] W.A. Little, The transport of heat between dissimilar solids at low temperatures, Can. J. Phys. 37 (1959) 334–349.
[24] E.T. Swartz, R.O. Pohl, Thermal boundary resistance, Rev. Mod. Phys. 61 (1989) 605–668.
[25] R. Prasher, Thermal conductivity of composites of aligned nanoscale and microscale wires and pores, J. Appl. Phys. 100 (2006) 034307.